Impact of anomalous Eurasian blocking activities on the East Asian Meiyu rainfall

Zitian Xu
Nanjing University

Xiu-Qun Yang (✉ xqyang@nju.edu.cn)
Nanjing University

Lingfeng Tao
Nanjing University

Linyuan Sun
Nanjing University

Abstract

An extreme East Asian Meiyu rainfall in both amount and duration occurred along Yangtze River valley during June-July of 2020, however, possible mid-high latitude signatures causing this super Meiyu have not been well identified. This study explores the cause of the Meiyu rainfall from the aspect of anomalous Eurasian blocking activities with a two-dimensional blocking index, using the Japanese 55-yr Reanalysis for 1979–2020. The major findings are as follows. Variabilities of the Eurasian blocking activities are primarily characterized by a tripole pattern with three centers over the Baltic Sea, the Ural Mountain, and the Sea of Okhotsk, respectively. The tripole pattern is associated with two zonally-oriented Rossby wavetrains which may originate from the rainfall anomaly in Central Europe. Corresponding to a positive phase of the tripole pattern, the northern wavetrain through energy dispersion tends to induce an anomalous anticyclone (i.e., enhanced blocking) over the Sea of Okhotsk, while the southern wavetrain tends to induce an anomalous cyclone over the Sea of Japan which is conducive to the southward intrusion of more high-latitude cold airs. Consequently, a meridional dipole anomalous circulation pattern over the northeastern Asia is formed, favoring more East Asian Meiyu rainfall. In 2020, the Eurasian blocking activities exhibit a significantly positive phase of the tripole pattern and considerably contribute to the super Meiyu. The results identified in this study highlight the importance of the Eurasian blocking activities in the East Asian Meiyu and provide a new perspective for the prediction of the Meiyu rainfall with mid-high latitude signatures.

1 Introduction

The unique East Asian rainy season from mid-June to mid-July is identified as Meiyu in China (Ding et al. 2020), Baiu in Japan (Ninomiya and Shibagaki 2007), and Changma in South Korea (Oh et al. 1997), which has attracted great attention from the international community in the past few decades (Ding et al. 2008; Li et al. 2008). The 2020 Meiyu rainfall is recognized as a 'super Meiyu' due to the strongest rainfall since the 1960s as well as an anomalous long duration (Liu et al. 2020a; Ding et al. 2021), In 2020, the severe flood exerts enormous impacts on the economic development and human life along the middle-lower reaches of the Yangtze River valley (YRV) in eastern China. Meanwhile, many regions throughout East Asia also experienced this historically extreme rainfall event (Takaya et al. 2020; Park et al. 2021; Wang et al. 2021). However, recent studies show that the commonly used signatures for the prediction of Meiyu are not significant in 2020 and could only explain part of this super Meiyu (Takaya et al. 2020; Zhou et al. 2021). Therefore, the physical mechanism responsible for the Meiyu rainfall is still a noteworthy research issue.

Previous studies highlight that the interannual variation of Meiyu rainfall is directly modulated by low latitude components of the East Asian summer monsoon (EASM), including the western Pacific subtropical high (WPSH) and the South Asian high (Zhou and Yu 2005; Wang et al. 2008; Ding et al. 2020). In particular, the intensified WPSH can enhance the northward transportation of water vapor from the tropical ocean to the YRV region. Moreover, the interannual variation of Meiyu rainfall is affected by sea surface temperature (SST) anomalies in the tropical Pacific and the Indian Ocean (Ding et al. 2008;

Feng et al. 2011; Kosaka et al. 2011; Xie et al. 2016; Takaya et al. 2020). Specifically, the impact of El Niño-Southern Oscillation (ENSO) on the East Asian Meiyu, which is associated with the developing or decaying phase of an ENSO event, also attracts extensive attention (Huang and Wu 1989; Chang et al. 2000; Fowler et al. 2008). As a significant predictor of the Meiyu rainfall, El Niño events generally lead to positive rainfall anomalies around the YRV in El Niño decaying summer (Sun et al. 2021). According to previous studies, the WPSH plays an important role in conveying the El Niño impact on the East Asian Meiyu rainfall (Li et al. 2017). In addition, the preceding winter El Niño has a close relationship with the warmer Indian ocean and leads to a positive rainfall anomaly in YRV through the impact on WPSH (Xie et al. 2016).

Although the above tropical anomalies can affect the Meiyu rainfall, those signatures are not in significant anomalous phases in 2020 and could only explain part of this super Meiyu (Takaya et al. 2020; Zhou et al. 2021). Compared with the tropical signatures, the extratropical signatures, which also play an important role in the EASM system, have been paid relatively little attention in previous studies. The Eurasian mid-to-high latitude large-scale circulation includes the Eurasian blocking activities, of which the Sea of Okhotsk blocking high can favor the southward intrusions of high-latitude cold-dry air into East Asia and thus enhance the Meiyu rainfall (Wang 1992; Li et al. 2001; Niu and Jin 2009; Li et al. 2010; Chen and Zhai 2014; Park and Ahn 2014). In 2020, the high-latitude blocking activities over East Siberia exert an important effect on the Meiyu-Baiu rainfall and result in this super Meiyu according to the recent studies (Chen et al. 2021; Ding et al. 2021).

Many previous studies explored the relationship between East Asian Meiyu and Eurasian blocking activities based on case studies (Wang 1992; Chen et al. 2007). Furthermore, to reflect the climatic effect of anomalous blocking activities on East Asian climate variabilities, several one-dimensional blocking indices are defined (Rex 1950; Dole 1978; Hartmann and Ghan 1980; Dole and Gordon 1983; Lejenäs and Økland 1983; Shukla and Mo 1983; Tibaldi and Molteni 1990; Lupo and Smith 1995). Among them, the T&M blocking index proposed by Tibaldi and Molteni (1990) has been widely used to reveal the zonal distribution of blocking activities. Two-dimensional blocking indices are further developed to reflect the two-dimensional spatial distribution of blocking highs (Pelly and Hoskins 2003; Diao et al. 2006; Davini et al. 2012; Masato et al. 2012; Kim and Ha 2015; Nakamura and Huang 2018), while they are seldom used to demonstrate the impact of blocking highs on the Meiyu rainfall in previous studies.

In this study, the effect of anomalous Eurasian blocking activities on the Meiyu rainfall on the interannual timescale is first explored with the two-dimensional blocking index proposed by Davini et al. (2012). Then, the atmospheric circulation anomalies associated with the anomalous Eurasian blocking activities are investigated from the view of quasi-stationary Rossby waves. In particular, the impact of anomalous Eurasian blocking activities on the Meiyu rainfall is used to explain the cause of super Meiyu in 2020. The rest of the paper is organized as follows. Section 2 describes the data and methods used in this study. Section 3 shows the characteristics of the leading mode of anomalous Eurasian blocking activities and the significant effect of this mode on the Meiyu rainfall. Section 4 illustrates the physical mechanisms responsible for the Eurasian blocking mode and its climate effect on East Asian precipitation. Section 5

analyzes the 2020 'super Meiyu' as a typical case to highlight the important impact of blocking high on the Meiyu rainfall. The final section is devoted to summary and discussion.

2 Data And Method

2.1 Data

To obtain the characteristic of precipitation during the Meiyu period, daily precipitation data with a 0.5°×0.5° horizontal resolution provided by NOAA Climate Prediction Center (CPC) is used in this study. The climatological time-latitude section (averaged between 110°E and 123°E) of summer (June, July, August, JJA in short) rainfall is shown in Fig. 1. The precipitation in eastern China mainly concentrates south of 28°N in early-June, and shifts northward gradually to the YRV afterward (area between the two red lines in Fig. 1). The rainband mainly locates in the YRV from mid-June to late-July. In August, the precipitation is decreased and the rainband becomes obscure. Therefore, based on the climatological evolution of the precipitation, the Meiyu period is defined as the months of June and July in this study. The time period is from 1979 to 2020, 42 years in total.

Daily atmospheric variables, including zonal and meridional winds, geopotential height, air temperature, and specific humidity at 27 standard pressure levels from 1000 to 100 hPa, as well as sea level pressure (SLP), are taken from the Japanese 55-yr Reanalysis (JRA-55), the second global atmospheric reanalysis conducted by the Japan Meteorological Agency with horizontal resolution at 1.25°×1.25° (Kobayashi et al. 2015; Harada et al. 2016). NCEP-NCAR Reanalysis dataset at 2.5° spatial resolution (Kalnay et al. 1996) is used to confirm the robustness of results. Daily solar radiative heating rate, longwave radiative heating rate, large-scale condensation heating rate, convective heating rate, and vertical diffusion heating rate from JRA-55 with the same resolution are used to calculate the total diabatic heating. Besides, daily radiative and surface turbulent heat flux, skin temperature, and air temperature at 2 m with a horizontal resolution of 1°×1° from the latest generation of ECMWF atmospheric reanalysis (ERA5) are used to diagnose the surface energy balance equation (Hersbach et al. 2020).

2.2 Method

The indices of blocking activities can be defined based on the type, lifetime, and other properties (Tibaldi and Molteni 1990; Scherrer et al. 2006). In this study, we focus on the frequency of blocking activities and choose to use the two-dimensional blocking index calculation developed by Scherrer et al. (2006) and Davini et al. (2012). This index is mainly defined based on the meridional gradient of 500 hPa geopotential height. For a given grid point (λ_0, Φ_0), the meridional gradient of 500 hPa geopotential height in its southern (GHGS) and northern (GHGN) flank is defined by:

$$\text{GHGS}\left(\lambda_0, \Phi_0\right) = \frac{\text{Z500}\left(\lambda_0, \Phi_0\right) - \text{Z500}\left(\lambda_0, \Phi_S\right)}{\Phi_0 - \Phi_S}$$

1

,

and $\mathrm{GHGN}\left(\lambda_0, \Phi_0\right) = \frac{Z500(\lambda_0, \Phi_N) - Z500(\lambda_0, \Phi_0)}{\Phi_N - \Phi_0}$, (2)

where λ_0 (Φ_0) denotes the longitude (latitude), Φ_S and Φ_N are the southern and northern boundary latitude defined as $\Phi_S = \Phi_0 - 15°$ and $\Phi_N = \Phi_0 + 15°$, respectively. The range of Φ_0 is 30°N to 75°N. When both $\mathrm{GHGS}\left(\lambda_0, \Phi_0\right) > 0$ and $\mathrm{GHGN}\left(\lambda_0, \Phi_0\right) < -10$, a local instantaneous blocking index (IB) is defined and set as one on that grid point, otherwise set as zero. The two-dimensional blocking index proposed by Diao et al. (2006) is also used to check the robustness of results.

The empirical orthogonal function (EOF) analysis (Lorenz 1956) is applied to extract the leading mode of the blocking frequency over the Eurasian continent (10°E-160°E, 45°N-75°N) during Meiyu period. Linear regression method is used to obtain the Eurasian blocking-related rainfall and atmospheric circulation anomalies. The statistical significance is assessed with Student's t-test. The Rossby wave source (Sardeshmukh and Hoskins 1988) and wave activity flux (WAF, Takaya and Nakamura 2001) are used to analyze the wave-related processes.

3 The Leading Mode Of Anomalous Eurasian Blocking Activities And Its Impacts On Meiyu Rainfall

In climatology, the spatial distributions of blocking frequency over Eurasian continent display three significant centers: the Baltic Sea blocking, the Ural Mountain blocking, and the Sea of Okhotsk blocking (Fig. 2a), which are also pointed by other studies (Li and Ding 2004; Park and Ahn 2014). The blocking frequencies in these blocking centers reach about 10 days per Meiyu period. Corresponding to the spatial distribution of blocking, the climatological atmospheric geopotential height over Eurasian continent is featured by a "two-ridge and one-trough" pattern during Meiyu period. Following Davini et al. (2012), more strict criteria on special scale (grids at least 15°continuous longitudes are blocked) and time persistence (last more than 5 days) are applied on IB to test the sensitivity. As shown in Fig. 2b, the spatial distribution of the strict blocking frequency basically is consistent with that of the pure IB index, albeit the amplitude is relatively weaker. To reduce possible discontinuity, the pure IB index is used here. Similar results (not shown) can be obtained based on the definition of blocking frequency by Diao et al. (2006).

Over the mid-to-high latitudes of Eurasian continent, the leading EOF mode of blocking frequency anomalies is featured by a tripole pattern during Meiyu period (Fig. 3a). Compared with the climatology (Fig. 2a), the Baltic Sea blocking and the Sea of Okhotsk blocking are significantly enhanced. The southern part of Ural Mountain blocking is enhanced and the northern part of it is weakened, indicating a southward movement of Ural Mountain blocking. The corresponding time series (tripole pattern index, TPI) explains 20.3% of the total variance and exhibits obvious year-to-year differences, indicating large variations of blocking frequency during Meiyu period on interannual timescale (bar in Fig. 3b).

Previous studies indicate that the blockings over the Eurasian continent may exert a significant influence on the East Asian Meiyu rainfall (Li and Ding 2004; Niu and Jin 2009; Chen et al. 2021; Ding et al. 2021). As shown in Fig. 4, corresponding to the positive phase of the tripole pattern of anomalous Eurasian blocking activities, the linearly regressed rainfall anomalies on TPI display a dipole pattern in East Asia: the precipitation is decreased along the Yellow River and northern Korean Peninsula, and is significantly increased over Yangtze River and its southern area, the southern Korean Peninsula and southern Japan. A Meiyu rainfall index (black lines in Fig. 4b) is defined by the standardized area-averaged (red box in Fig. 4a) precipitation anomalies during Meiyu period. The year-to-year change of Meiyu rainfall anomaly resembles to that of the tripole blocking frequency anomalies, especially in recent three decades (black line vs. bar in Fig. 4b). The 42-year correlation coefficient between the Meiyu index and TPI is 0.40 (passes the Student's t-test at 0.05 significant level), showing that there exists a possible close relationship between the tripole pattern of Eurasian blocking activities and the Meiyu rainfall anomaly. Noticeably, the Meiyu index in 2020 is outstanding and exceeds 4.0 standard deviations, which is the highest in the past 40 years. Meanwhile, TPI reaches about 1.0 standard deviation, indicating a strong positive tripole pattern of Eurasian blocking activities occurs in the year 2020.

Similarly, through linear regression upon TPI, the atmospheric anomalies that are related with the positive phase of the tripole pattern of anomalous Eurasian blocking activities during Meiyu period are obtained (Fig. 5). During the positive phase of the tripole pattern, there is an atmospheric cyclonic wind anomaly around the Yellow Sea and an anticyclonic wind anomaly over the South China Sea on 850 hPa (vectors in Fig. 5b). Consequently, the moisture flux is convergent between 20°N and 30°N in eastern Asia (shaded in Fig. 5a), supporting the increased rainfall anomaly there (Fig. 4a). Meanwhile, the Yellow River and its northern area are controlled by 850 hPa cold temperature advection anomaly, and the south flank of 30°N in East Asian continent is controlled by warm temperature advection anomaly (shaded in Fig. 5b). The cold air from mid-to-high latitudes and the warm air from lower latitudes are against to each other over the YRV, which enhances the meridional temperature gradient and favors the persistent rainfall there. Therefore, influenced by both mid-to-high latitudes and the lower latitudes, the rainfall over southern East Asia is increased during Meiyu Period.

4 Dynamical Analysis On The Relationship Between Eurasian Blocking Activities And Meiyu Rainfall

Over the midlatitude Eurasian continent, the Rossby waves play important roles in connecting remote atmospheric anomalies (Enomoto 2004; Chowdary et al. 2019; Li et al. 2021a; Wang et al. 2017). Accordingly, the TPI-related upper-level WAF, Rossby wave source, and corresponding geopotential height anomalies are shown in Fig. 6. Corresponding to the tripole anomaly of Eurasian blocking activities, the geopotential height anomalies are higher than climatology over Ural area, Mongolia area, and Far East area, and are lower in Central Europe, Central Asia, Sea of Japan, Kara Sea, and northwest of North Pacific (shade in Fig. 6a), among which Central Europe is an important source of the Rossby waves (shaded in Fig. 6b).

The Rossby wavetrains that are related with the tripole pattern of anomalous Eurasian blocking activities, basically propagate along two zonally-oriented pathways: the northern branch propagates northeastward to Ural area and Kara Sea, then southeastward to the Far East and arrives the northwest of North Pacific, and the southern branch propagates to the south of Ural area, then southeastward to Central Asia and Mongolia area, and reaches the Korean Peninsula. The former and the latter route are defined as the northern and southern propagation pathways, respectively. For both two pathways that are related with the tripole pattern of anomalous Eurasian blocking activities, the amplified WAF over the Ural area is important. The northerly pathway locates in mid-to-high latitudes, and tends to enhance the Sea of Okhotsk blocking. Meanwhile, the southern pathway locates mainly in midlatitudes, and tends to induce a negative geopotential height anomaly over the Sea of Japan (Fig. 6a). The corresponding northerly wind of the cyclonic circulation over East Asia helps the transportation of cold/dry air from high to lower latitudes (Fig. 5), which in favor of the formation of rainfall over YRV. Some recent studies also pointed out that the Rossby wavetrain from Europe could affect the climate in East Asia, such as the Silk Road pattern (Wang et al. 2017; Liu et al. 2020b), and the British-Okhotsk Corridor pattern (Li et al. 2021b; Xu et al. 2022).

To explore the causation of the anomalous Rossby wave source in Central Europe, Fig. 7 shows the total diabatic heating anomaly over the Central Europe in vertical direction and its components, including vertical diffusion, latent heat from convective processes and large-scale condensation, longwave and shortwave radiation. The diabatic heating anomaly over Central Europe is positive between 700 hPa-300 hPa and negative below 700 hPa (Fig. 7a). The vertical distribution of diabatic heating anomalies is mainly induced by the moisture condensation latent heat released from convective processes (Fig. 7c), albeit the longwave radiation partly contributes to the low-level diabatic cooling anomaly (Fig. 7e). From the view of horizontal distribution (Fig. 8), during positive phase of the tripole pattern of anomalous Eurasian blocking activities, the precipitation anomaly as well as the diabatic heating anomaly is increased around Central Europe (Fig. 8a, b). The similar horizontal distributions of regressed precipitation and vertically integrated diabatic heating support again that the diabatic heating anomalies are mainly induced by moisture condensation. Resultantly, the atmospheric circulation displays a divergent field in high-level troposphere, which conduce to the formation of the Rossby wave source there.

In order to verify the remote relationship between Central Europe rainfall and Meiyu rainfall, a Central Europe rainfall index is defined by the area-mean precipitation in Central Europe (red box in Fig. 8a). As shown in Fig. 4b, the correlation coefficient between the Meiyu rainfall index and the Central Europe precipitation index (black vs. purple lines in Fig. 4b) is 0.34, which passes the Student's t-test at 0.05 significant level. Similarly, linear regressions of atmospheric variables upon the standardized Central Europe precipitation index are employed. When the rainfall anomaly in Central Europe is increased (Fig. 9a), the atmospheric diabatic heating is anomalously positive (Fig. 9b) and leads an anomalous upper-level divergence (Fig. 9c), which tends to excite a Rossby wave source (Fig. 10c). Correspondingly, the Rossby wave propagations present as a wavetrain in European area and branches into two part in the downstream of Ural area (Fig. 10b, c), which are similar to those two Rossby wavetrains that are associated with the tripole pattern of anomalous Eurasian blocking activities (Fig. 6b). The northern

Rossby wavetrain strengthens the blocking highs over the Europe area and to the north of the Sea of Okhotsk (Fig. 10a), which resembles the tripole pattern (Fig. 3a). Meanwhile, the southern Rossby wavetrain tends to induce a negative geopotential height anomaly over the Korean Peninsula and East China Sea, which tends to transport cold/dry to the north of YRV (Fig. 11c) and leads the convergent atmospheric moisture flux anomaly around the YRV (Fig. 11b). Resultantly, the rainfall in the YRV and south of Japan is anomalously increased during Meiyu Period.

Except for the formation of the Rossby wave source over Central Europe, the largely amplified WAF over the Ural area is also essential for both pathways as mentioned before. Previous studies noticed that the local surface processes are important in the formation and maintenance of Ural blocking activities (Seneviratne et al. 2010; Zhang et al. 2018b). Figure 12 illustrates the regressed variables of the surface energy balance equation, including surface shortwave and longwave radiation, surface turbulent sensible and latent heat flux, air-land temperature differences (skin temperature minus 2 m temperature), and skin temperature onto TPI. Taking the Ural area as an example (the leftmost red box in Fig. 12), when the geopotential height over the Ural area is anomalously high, the downward net shortwave radiation is increased and warms the surface (Fig. 12a, f). The resultant upward longwave radiation, sensible and latent heat flux (Fig. 12c, d) anomaly induce a positive diabatic heating anomaly in the boundary layer, which leads to a negative vertical gradient anomaly of diabatic heating. According to the quasi-geostrophic potential vorticity equation in midlatitudes (Fang and Yang 2016; Tao et al. 2019; Tao et al. 2020), the negative vertical gradient anomaly of diabatic heating tends to maintain the positive geopotential height anomaly near surface, and thus forms a local positive feedback.

Similar to the positive feedback in the Ural area, the geopotential anomalies over Mongolia, Siberian Plateau, and the Far East also tend to be strengthened by the air-land interactions, which can amplify the WAF and support the transportation of atmospheric perturbation. On this regard, the local air-land interaction acts as a "gas station" during the propagation of the Rossby wavetrains. The existence of "gas stations" may explain why the atmospheric perturbation over Central Europe could be powerful enough to be transported to the North Pacific region, and influence the Meiyu rainfall efficiently. The detailed processes will be investigated further in our future work.

5 Case Analysis On 2020 Super Meiyu Event

In sections 3 and 4, the impact of anomalous Eurasian blocking activities on Meiyu rainfall and the physical processes in it are investigated by regression method. As mentioned before, the Meiyu rainfall in the YRV reaches its highest value in 2020. In this section, the 2020 super Meiyu event is taken as a case to analyze how the Eurasian blocking activities contribute to the super Meiyu.

During the 2020 Meiyu period, rainfall anomaly largely increased around the YRV and south Japan, of which the maximum value exceeded 20 mm day^{-1}. The distribution of precipitation anomaly in 2020 (Fig. 13a) closely resembles to that of the regression upon TPI (Fig. 4a) and Central Europe precipitation index (Fig. 11a). Although the cyclonic wind anomaly in the Korean Peninsula is relatively feeble, the

northly wind of it in favor of the atmospheric moisture flux convergence locates over the YRV (Fig. 13b) and the cold air temperature advection in the north of the YRV (Fig. 13c), which helps the Meiyu rainfall stay along the YRV.

During the 2020 Meiyu period, the TPI index and Central Europe precipitation index are near 1.0 standard deviation and 1.5 standard deviations, respectively. The Eurasian blocking activities in 2020 are anomalously strengthened over the Baltic Sea blocking, the south of the Ural Mountain blocking, and the north of the Sea of Okhotsk blocking (Fig. 14a), basically displaying the tripole distribution (Fig. 3a). The precipitation anomaly is largely increased over Central Europe (Fig. 15a), inducing a positive diabatic heating anomaly (Fig. 15b). Consequently, the atmospheric circulations are divergent in high-level tropopause (Fig. 15c), which leads a Rossby wave source there (Fig. 14c). The propagations of Rossby wave anomalies in 2020 resemble to that of regression upon TPI (Fig. 6) and Central Europe precipitation index (Fig. 10), namely the Rossby wave energy originates from Central Europe and propagates eastward through northern and southern these two pathways (Fig. 14b, c). Therefore, although the tropical influence may be the primary causation for the record-breaking Meiyu rainfall anomaly in 2020, the mid-to-high latitude anomalies provide a favorable condition for the large amount and long persistence of the heavy rainfall.

6 Summary And Discussion

During June-July of 2020, a record-breaking East Asian Meiyu rainfall occurred around the Yangtze River valley. A number of studies indicate that tropical air-sea anomalies play an important role in the formation of extreme Meiyu rainfall. However, the impact of mid-to-high latitude anomalies on this super Meiyu rainfall is still an open question. In this study, the cause of Meiyu rainfall is explored from the aspect of anomalous Eurasian blocking activities.

Based on the JRA-55 reanalysis dataset from 1979 to 2020, the anomalous Eurasian blocking activities are represented by a two-dimensional blocking index. The leading EOF mode of the anomalous Eurasian blocking activities during Meiyu period shows a tripole pattern with three positive centers located in Baltic Sea, Ural Mountain, and Sea of Okhotsk, respectively. As illustrated in the schematic diagram (Fig. 16), the tripole pattern is associated with two zonally-oriented Rossby wavetrains that are excited by the rainfall anomaly in Central Europe. Corresponding to the positive phase of the tripole pattern, the northern wavetrain through energy dispersion tends to induce an anomalous geopotential high over the Sea of Okhotsk, and the southern wavetrain tends to induce an anomalous geopotential low over Sea of Japan. The anomalous cyclonic circulation over Sea of Japan leads a southward intrusion of more high-latitude cold airs, and helps to increase East Asian Meiyu rainfall.

During the 2020 Meiyu period, the anomalous Eurasian blocking activities exhibit a significant positive tripole pattern. The precipitation anomaly in Central Europe is largely increased, inducing more diabatic heating anomaly and leads to the formation of a Rossby wave source there. Induced by the two zonally-oriented Rossby wavetrains from Central Europe, more high-latitude cold-dry airs are transported

southward to lower midlatitudes, which increase the Meiyu rainfall in East Asia. Although the tropical influence may be the primary reason for the record-breaking Meiyu rainfall anomaly, the Eurasian blocking activities make considerably contribution to the super Meiyu. The mid-to-high latitude anomalies provide a favorable condition for the large amount and long persistence of the heavy Meiyu rainfall. In this regard, the results provide a new perspective for the prediction of Meiyu rainfall by using mid-to-high latitude signals.

In this study, the impact of the Eurasian blocking activities on East Asian Meiyu rainfall is highlighted. Previous studies indicate that the anomalous Eurasian blocking activities may be related with the early spring Arctic sea ice cover (Wu et al. 2013; Petrie et al. 2015; Zhang et al. 2018a; Zhang et al. 2018b), the sub-seasonal phase transition of the North Atlantic Oscillation (Luo et al. 2015; Luo et al. 2016; Liu et al. 2020a), and a tripole sea surface temperature pattern in the North Atlantic (Wu et al. 2009; Wu et al. 2011; Zuo et al. 2013). Lead-lag analysis should be applied to explore the factors that contribute to the formation of the tripole pattern of the anomalous Eurasian blocking activities during Meiyu period. In addition, the results show that the precipitation in Central Europe can influence the remote East Asian Meiyu rainfall through two zonally-oriented Rossby wavetrains. Some recent studies also pointed out that the European anomalies could affect the climate in East Asia by long-distance Rossby wavetrains (Liu et al. 2020b; Li et al. 2021b; Wang et al. 2017; Xu et al. 2022). Based on this study, the Rossby wavetrains are enhanced by the local air-land processes. The positive feedbacks act as "gas stations", which favors the maintenance of the local atmospheric anomalies and support the long-distance downstream energy dispersion efficiently. The detailed processes in it still need further investigation, however, which are beyond the scope of this study.

Declarations

Ethics approval and consent to participate

The authors follow the rules of good scientific practice.

Consent for publication

Written informed consent for publication was obtained from all participants.

Availability of data and material

The Japanese 55-year Reanalysis (JRA-55) data was provided by the Japan Meteorological Agency and is available at https://rda.ucar.edu. The daily precipitation data was produced by NOAA Climate Prediction Center (CPC) and can be obtained from https://psl.noaa.gov/data/gridded/data.cpc.globalprecip.html. The fifth generation ECMWF reanalysis (ERA-5) data was produced by ECMWF and is available from https://www.ecmwf.int/en/forecasts/datasets. The NCEP-NACR Reanalysis 1 (NCEP-1) is available at http://www.esrl.noaa.gov/psd/data/gridded/data.ncep.reanalysis.html.

References

1. Chang CP, Zhang Y, Li T (2000) Interannual and interdecadal variations of the East Asian summer monsoon and tropical Pacific SSTs. Part I : Role of the subtropical ridge. Journal of Climate 13:4310-4325. https://doi.org/10.1175/1520-0442(2000)013<4310:IAIVOT>2.0.CO;2

2. Chen GT-J, Wang C-C, Wang A-H (2007) A case study of subtropical frontogenesis during a blocking event. Monthly weather review 135:2588-2609. https://doi.org/10.1175/MWR3412.1

3. Chen X, Dai A, Wen Z, Song Y (2021) Contributions of Arctic sea-ice loss and East Siberian atmospheric blocking to 2020 record-breaking Meiyu-Baiu rainfall. Geophysical Research Letters 48:e2021GL092748. https://doi.org/10.1029/2021GL092748

4. Chen Y, Zhai P (2014) Two types of typical circulation pattern for persistent extreme precipitation in Central−Eastern China. Quarterly Journal of the Royal Meteorological Society 140:1467-1478. https://doi.org/10.1002/qj.2231

5. Chowdary JS, Hu K, Srinivas G, Kosaka Y, Wang L, Rao KK (2019) The Eurasian jet streams as conduits for East Asian monsoon variability. Current Climate Change Reports 5:233-244. https://doi.org/10.1007/s40641-019-00134-x

6. Davini P, Cagnazzo C, Gualdi S, Navarra A (2012) Bidimensional diagnostics, variability, and trends of Northern Hemisphere blocking. Journal of Climate 25:6496-6509. https://doi.org/10.1175/JCLI-D-12-00032.1

7. Diao Y, Li J, Luo D (2006) A New Blocking Index and Its Application: Blocking Action in the Northern Hemisphere. Journal of Climate 19:4819-4839. https://doi.org/10.1175/JCLI3886.1

8. Ding Y, Liang P, Liu Y, Zhang Y (2020) Multiscale variability of Meiyu and its prediction: A new review. Journal of Geophysical Research: Atmospheres 125:e2019JD031496. https://doi.org/10.1029/2019JD031496

9. Ding Y, Liu Y, Hu Z-Z (2021) The record-breaking mei-yu in 2020 and associated atmospheric circulation and tropical SST anomalies. Advances in Atmospheric Sciences 38:1980-1993. 10.1007/s00376-021-0361-2

10. Ding Y, Wang Z, Sun Y (2008) Inter-decadal variation of the summer precipitation in East China and its association with decreasing Asian summer monsoon. Part I: Observed evidences. International Journal of Climatology: A Journal of the Royal Meteorological Society 28:1139-1161. https://doi.org/10.1002/joc.1615

11. Dole R (1978) The objective representation of blocking patterns. The general circulation: theory, modeling and observations:406-426

12. Dole RM, Gordon ND (1983) Persistent anomalies of the extratropical Northern Hemisphere wintertime circulation: Geographical distribution and regional persistence characteristics. Monthly Weather Review 111:1567-1586. https://doi.org/10.1175/1520-0493(1983)111<1567:PAOTEN>2.0.CO;2

13. Enomoto T (2004) Interannual variability of the Bonin high associated with the propagation of Rossby waves along the Asian jet. Journal of the Meteorological Society of Japan Ser II 82:1019-1034. https://doi.org/10.2151/jmsj.2004.1019

14. Fang J, Yang X-Q (2016) Structure and dynamics of decadal anomalies in the wintertime midlatitude North Pacific ocean–atmosphere system. Climate Dynamics 47:1989-2007. 10.1007/s00382-015-2946-x

15. Feng J, Chen W, Tam CY, Zhou W (2011) Different impacts of El Niño and El Niño Modoki on China rainfall in the decaying phases. International Journal of Climatology 31:2091-2101. https://doi.org/10.1002/joc.2217

16. Fowler AM, Boswijk G, Gergis J, Lorrey A (2008) ENSO history recorded in Agathis australis (kauri) tree rings. Part A: kauri's potential as an ENSO proxy. International Journal of Climatology: A Journal of the Royal Meteorological Society 28:1-20. https://doi.org/10.1002/joc.1525

17. Harada Y et al. (2016) The JRA-55 Reanalysis: Representation of atmospheric circulation and climate variability. Journal of the Meteorological Society of Japan Ser II 94:269-302. https://doi.org/10.2151/jmsj.2016-015

18. Hartmann DL, Ghan SJ (1980) A statistical study of the dynamics of blocking. Monthly Weather Review 108:1144-1159. https://doi.org/10.1175/1520-0493(1980)108<1144:ASSOTD>2.0.CO;2

19. Hersbach H et al. (2020) The ERA5 global reanalysis. Quarterly Journal of the Royal Meteorological Society 146:1999-2049. https://doi.org/10.1002/qj.3803

20. Huang R, Wu Y (1989) The Influence of ENSO on the Summer Climate Change in China and Its Mechanism. Advances in Atmospheric Sciences 6:21-32

21. Kalnay E et al. (1996) The NCEP/NCAR 40-year reanalysis project. Bulletin of the American meteorological Society 77:437-472. https://doi.org/10.1175/1520-0477(1996)077<0437:TNYRP>2.0.CO;2

22. Kim S-H, Ha K-J (2015) Two leading modes of Northern Hemisphere blocking variability in the boreal wintertime and their relationship with teleconnection patterns. Climate Dynamics 44:2479-2491. 10.1007/s00382-014-2304-4

23. Kobayashi S, Coauthors (2015) The JRA-55 reanalysis: general specifications and basic characteristics. Journal of the Meteorological Society of Japan Ser II 93:5-48. https://doi.org/10.2151/jmsj.2015-001

24. Kosaka Y, Xie S-P, Nakamura H (2011) Dynamics of interannual variability in summer precipitation over East Asia. Journal of Climate 24:5435-5453. https://doi.org/10.1175/2011JCLI4099.1

25. Lejenäs H, Økland H (1983) Characteristics of Northern Hemisphere blocking as determined from a long time series of observational data. Tellus A 35:350-362. https://doi.org/10.1111/j.1600-0870.1983.tb00210.x

26. Li CY, Gu W, Pan J (2008) Mei-yu, Arctic Oscillation and Stratospheric Circulation Anomalies. Chinese Journal of Geophysics 51:1127-1135. https://doi.org/10.1002/cjg2.1308

27. Li F, Ding Y (2004) Statistical characteristic of atmospheric blocking in the Eurasia high-mid latitudes based on recent 30-year summers. Acta Meteor Sin 62:347-354

28. Li Q, Zhao M, Yang S, Shen X, Dong L, Liu Z (2021a) A zonally-oriented teleconnection pattern induced by heating of the western Tibetan Plateau in boreal summer. Climate Dynamics 57:2823-2842. 10.1007/s00382-021-05841-6

29. Li S, Ji L, Lin W, Ni Y (2001) The maintenance of the blocking over the Ural Mountains during the second Meiyu period in the summer of 1998. Advances in Atmospheric Sciences 18:87-105. 10.1007/s00376-001-0006-4

30. Li T, Wang B, Wu B, Zhou T, Chang C-P, Zhang R (2017) Theories on formation of an anomalous anticyclone in western North Pacific during El Niño: A review. Journal of Meteorological Research 31:987-1006. 10.1007/s13351-017-7147-6

31. Li X, Lu R, Ahn J-B (2021b) Combined effects of the British–Baikal Corridor pattern and the Silk Road pattern on Eurasian surface air temperatures in summer. Journal of Climate 34:3707-3720. https://doi.org/10.1175/JCLI-D-20-0325.1

32. Li Y, Jin R-h, Wang S-g (2010) Possible relationship between ENSO and blocking in key regions of Eurasia. Journal of Tropical Meteorology 16:221

33. Liu B, Yan Y, Zhu C, Ma S, Li J (2020a) Record-breaking Meiyu rainfall around Yangtze River in 2020 regulated by the subseasonal phase transition of North Atlantic Oscillation. https://doi.org/10.1029/2020GL090342

34. Liu Y, Zhou W, Qu X, Wu R (2020b) An interdecadal change of the boreal summer Silk Road pattern around the late 1990s. Journal of Climate 33:7083-7100. https://doi.org/10.1175/JCLI-D-19-0795.1

35. Lorenz EN (1956) Empirical orthogonal functions and statistical weather prediction vol 1. Massachusetts Institute of Technology, Department of Meteorology Cambridge,

36. Luo D, Xiao Y, Diao Y, Dai A, Franzke CL, Simmonds I (2016) Impact of Ural blocking on winter warm Arctic–cold Eurasian anomalies. Part II: The link to the North Atlantic Oscillation. Journal of Climate 29:3949-3971. https://doi.org/10.1175/JCLI-D-15-0612.1

37. Luo D, Yao Y, Dai A (2015) Decadal relationship between European blocking and the North Atlantic Oscillation during 1978–2011. Part I: Atlantic conditions. Journal of the atmospheric sciences 72:1152-1173. https://doi.org/10.1175/JAS-D-14-0039.1

38. Lupo AR, Smith PJ (1995) Climatological features of blocking anticyclones in the Northern Hemisphere. Tellus A 47:439-456. https://doi.org/10.1034/j.1600-0870.1995.t01-3-00004.x

39. Masato G, Hoskins B, Woollings TJ (2012) Wave-breaking characteristics of midlatitude blocking. Quarterly Journal of the Royal Meteorological Society 138:1285-1296. https://doi.org/10.1002/qj.990

40. Nakamura N, Huang CS (2018) Atmospheric blocking as a traffic jam in the jet stream. Science 361:42-47. 10.1126/science.aat072

41. Ninomiya K, Shibagaki Y (2007) Multi-Scale Features of the Meiyu-Baiu Front and Associated Precipitation Systems. Journal of the Meteorological Society of Japan 85B:103-122. https://doi.org/10.2151/jmsj.85B.103

42. Niu R, Jin R (2009) Causes analysis of large scale circulation of abnormal characteristics in Meiyu period of 2008. Plateau Metorology 28:1326-1334

43. Oh J-H, Kwon W-T, Ryoo S-B (1997) Review of the researches on Changma and future observational study (KORMEX). Advances in Atmospheric Sciences 14:207-222. 10.1007/s00376-997-0020-2

44. Park C et al. (2021) Record-breaking summer rainfall in South Korea in 2020: Synoptic characteristics and the role of large-scale circulations. Monthly Weather Review 149:3085-3100. https://doi.org/10.1175/MWR-D-21-0051.1

45. Park YJ, Ahn JB (2014) Characteristics of atmospheric circulation over East Asia associated with summer blocking. Journal of Geophysical Research: Atmospheres 119:726-738. https://doi.org/10.1002/2013JD020688

46. Pelly JL, Hoskins BJ (2003) A new perspective on blocking. Journal of the atmospheric sciences 60:743-755. https://doi.org/10.1175/1520-0469(2003)060<0743:ANPOB>2.0.CO;2

47. Petrie RE, Shaffrey LC, Sutton R (2015) Atmospheric response in summer linked to recent Arctic sea ice loss. Quarterly Journal of the Royal Meteorological Society 141:2070-2076. https://doi.org/10.1002/qj.2502

48. Rex DF (1950) Blocking action in the middle troposphere and its effect upon regional climate. Tellus 2:275-301

49. Sardeshmukh PD, Hoskins BJ (1988) The generation of global rotational flow by steady idealized tropical divergence. Journal of the Atmospheric Sciences 45:1228-1251

50. Scherrer SC, Croci-Maspoli M, Schwierz C, Appenzeller C (2006) Two-dimensional indices of atmospheric blocking and their statistical relationship with winter climate patterns in the Euro-Atlantic region. International Journal of Climatology: A Journal of the Royal Meteorological Society 26:233-249

51. Seneviratne SI et al. (2010) Investigating soil moisture–climate interactions in a changing climate: A review. Earth-Science Reviews 99:125-161. https://doi.org/10.1016/j.earscirev.2010.02.004

52. Shukla J, Mo K (1983) Seasonal and geographical variation of blocking. Monthly Weather Review 111:388-402. https://doi.org/10.1175/1520-0493(1983)111<0388:SAGVOB>2.0.CO;2

53. Sun L, Yang X-Q, Tao L, Fang J, Sun X (2021) Changing Impact of ENSO Events on the Following Summer Rainfall in Eastern China since the 1950s. Journal of Climate 34:8105-8123. https://doi.org/10.1175/JCLI-D-21-0018.1

54. Takaya K, Nakamura H (2001) A formulation of a phase-independent wave-activity flux for stationary and migratory quasigeostrophic eddies on a zonally varying basic flow. Journal of the Atmospheric Sciences 58:608-627

55. Takaya Y, Ishikawa I, Kobayashi C, Endo H, Ose T (2020) Enhanced Meiyu-Baiu rainfall in early summer 2020: Aftermath of the 2019 super IOD event. Geophysical Research Letters 47:e2020GL090671. https://doi.org/10.1029/2020GL090671

56. Tao L, Sun X, Yang XQ (2019) The asymmetric atmospheric response to the midlatitude North Pacific SST anomalies. Journal of Geophysical Research: Atmospheres 124:9222-9240. https://doi.org/10.1029/2019JD030500

57. Tao L, Yang X-Q, Fang J, Sun X (2020) PDO-related wintertime atmospheric anomalies over the midlatitude North Pacific: local versus remote SST forcing. Journal of Climate 33:6989-7010. https://doi.org/10.1175/JCLI-D-19-0143.1

58. Tibaldi S, Molteni F (1990) On the operational predictability of blocking. Tellus A 42:343-365. https://doi.org/10.1034/j.1600-0870.1990.t01-2-00003.x

59. Wang B, Wu Z, Li J, Liu J, Chang C-P, Ding Y, Wu G (2008) How to measure the strength of the East Asian summer monsoon. Journal of Climate 21:4449-4463. https://doi.org/10.1175/2008JCLI2183.1

60. Wang L, Sun X, Yang X, Tao L, Zhang Z (2021) Contribution of water vapor to the record-breaking extreme Meiyu rainfall along the Yangtze River valley in 2020. Journal of Meteorological Research 35:557-570. 10.1007/s13351-021-1030-1

61. Wang L, Xu P, Chen W, Liu Y (2017) Interdecadal variations of the Silk Road pattern. Journal of Climate 30:9915-9932. https://doi.org/10.1175/JCLI-D-17-0340.1

62. Wang Y (1992) Effects of blocking anticyclones in Eurasia in the rainy season (Meiyu/Baiu season). Journal of the Meteorological Society of Japan Ser II 70:929-951. https://doi.org/10.2151/jmsj1965.70.5_929

63. Wu B, Zhang R, D'Arrigo R, Su J (2013) On the relationship between winter sea ice and summer atmospheric circulation over Eurasia. Journal of Climate 26:5523-5536. https://doi.org/10.1175/JCLI-D-12-00524.1

64. Wu R, Yang S, Liu S, Sun L, Lian Y, Gao Z (2011) Northeast China summer temperature and north Atlantic SST. Journal of Geophysical Research: Atmospheres 116. https://doi.org/10.1029/2011JD015779

65. Wu Z, Wang B, Li J, Jin FF (2009) An empirical seasonal prediction model of the East Asian summer monsoon using ENSO and NAO. Journal of Geophysical Research: Atmospheres 114. https://doi.org/10.1029/2009JD011733

66. Xie S-P, Kosaka Y, Du Y, Hu K, Chowdary JS, Huang G (2016) Indo-western Pacific Ocean capacitor and coherent climate anomalies in post-ENSO summer: A review. Advances in Atmospheric Sciences 33:411-432. 10.1007/s00376-015-5192-6

67. Xu P, Wang L, Dong Z, Li Y, Shen X, Chen W (2022) The British-Okhotsk Corridor pattern and its linkage to the Silk Road pattern. Journal of Climate:1-39. https://doi.org/10.1175/JCLI-D-21-0705.1

68. Zhang R, Sun C, Li W (2018a) Relationship between the interannual variations of Arctic sea ice and summer Eurasian teleconnection and associated influence on summer precipitation over China. Chinese Journal of Geophysics 61:91-105. 10.6038/cjg2018K0755

69. Zhang R, Sun C, Zhang R, Jia L, Li W (2018b) The impact of Arctic sea ice on the inter-annual variations of summer Ural blocking. International Journal of Climatology 38:4632-4650. https://doi.org/10.1002/joc.5731

70. Zhou TJ, Yu RC (2005) Atmospheric water vapor transport associated with typical anomalous summer rainfall patterns in China. Journal of Geophysical Research: Atmospheres 110. https://doi.org/10.1029/2004JD005413

71. Zhou Z-Q, Xie S-P, Zhang R (2021) Historic Yangtze flooding of 2020 tied to extreme Indian Ocean conditions. Proceedings of the National Academy of Sciences 118. https://doi.org/10.1073/pnas.2022255118

72. Zuo J, Li W, Sun C, Xu L, Ren H-L (2013) Impact of the North Atlantic sea surface temperature tripole on the East Asian summer monsoon. Advances in Atmospheric Sciences 30:1173-1186. 10.1007/s00376-012-2125-5
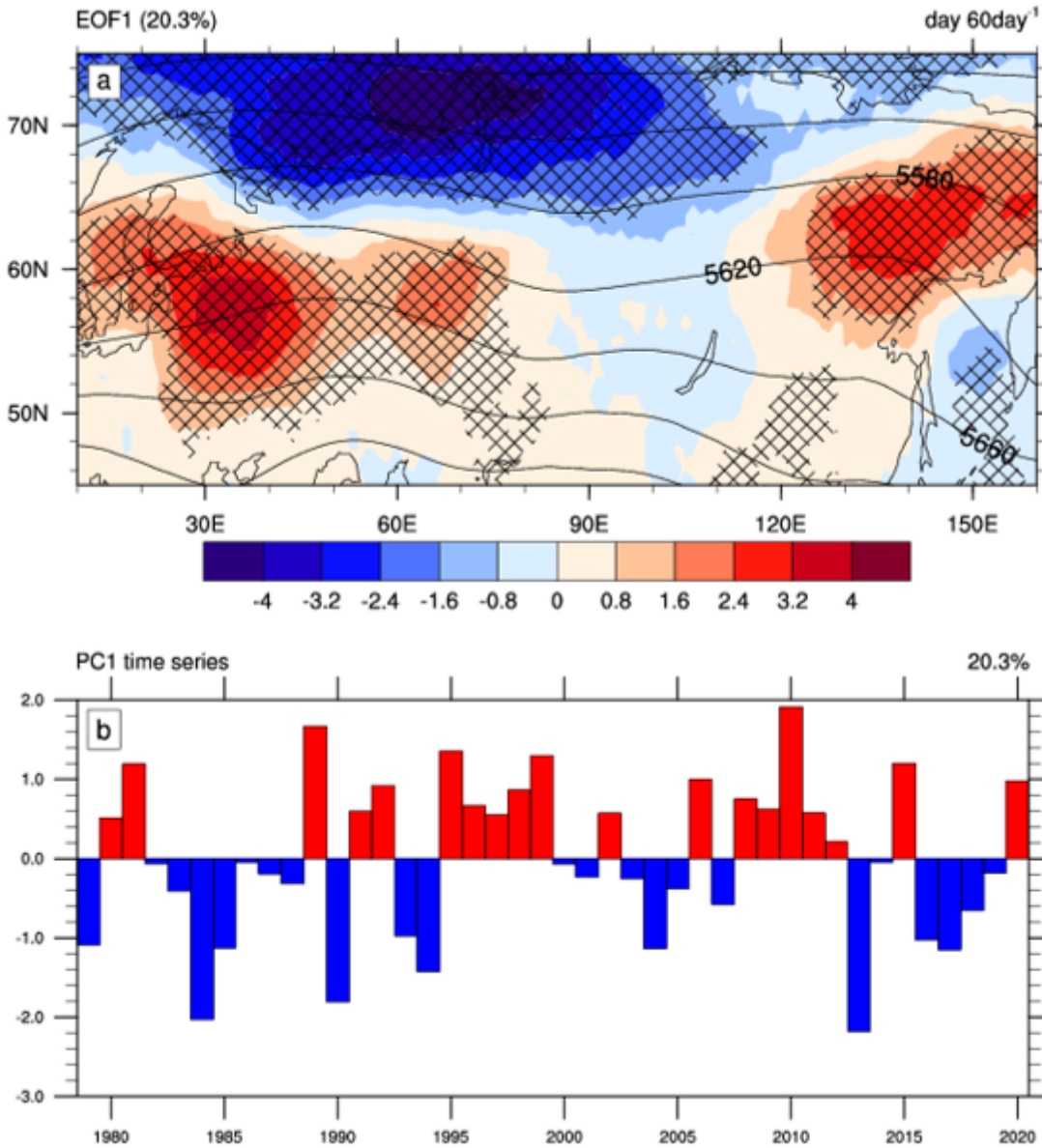
Figures
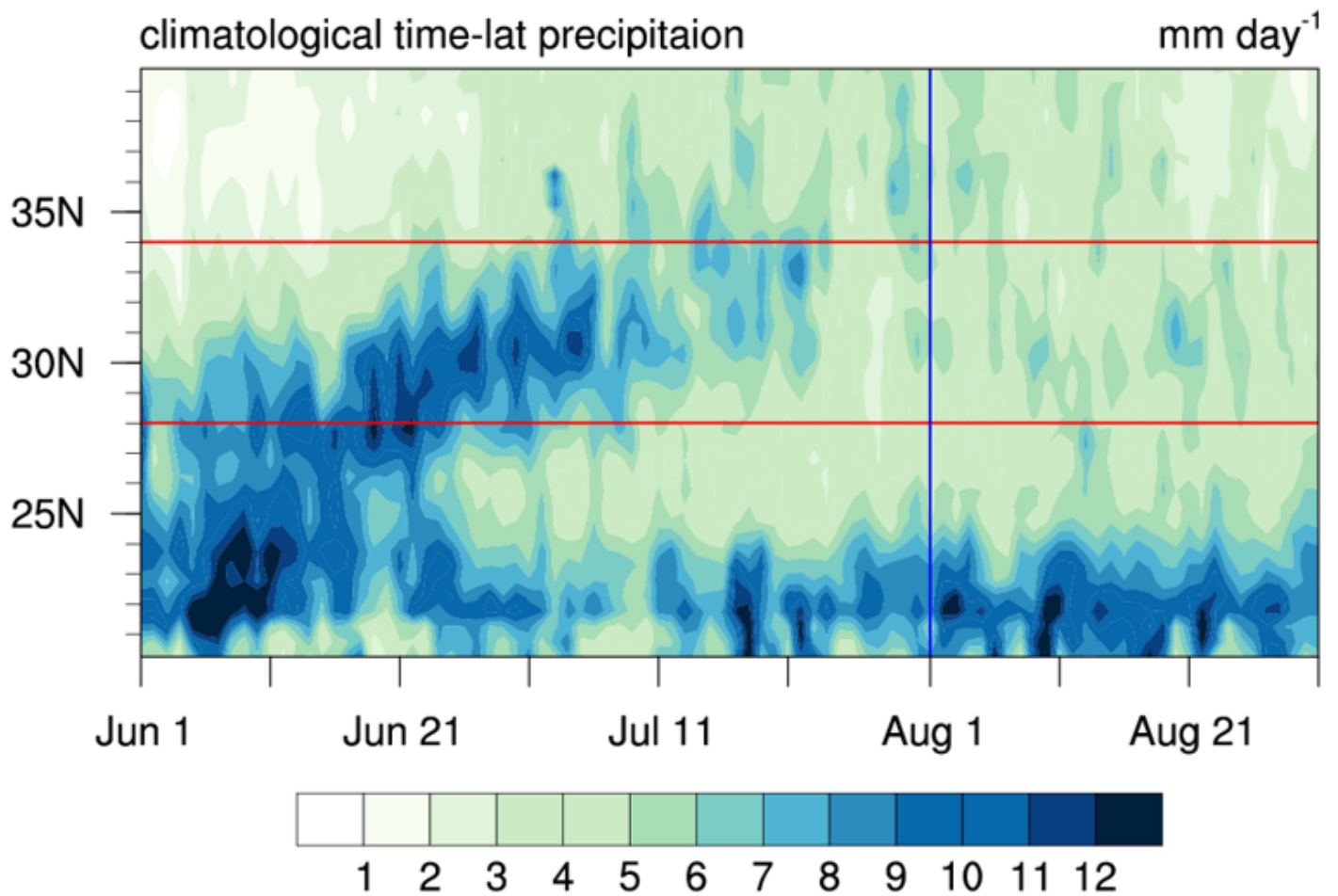
Figure 1

Time-latitude section of the zonal-averaged (110°E-123°E) climatological summer (JJA) rainfall (units: mm day^{-1}). The red lines denote the latitudes 28°N and 34°N, respectively. The area between the red lines represents the latitude of Yangtze River valley. The blue line represents the day of August 1st.
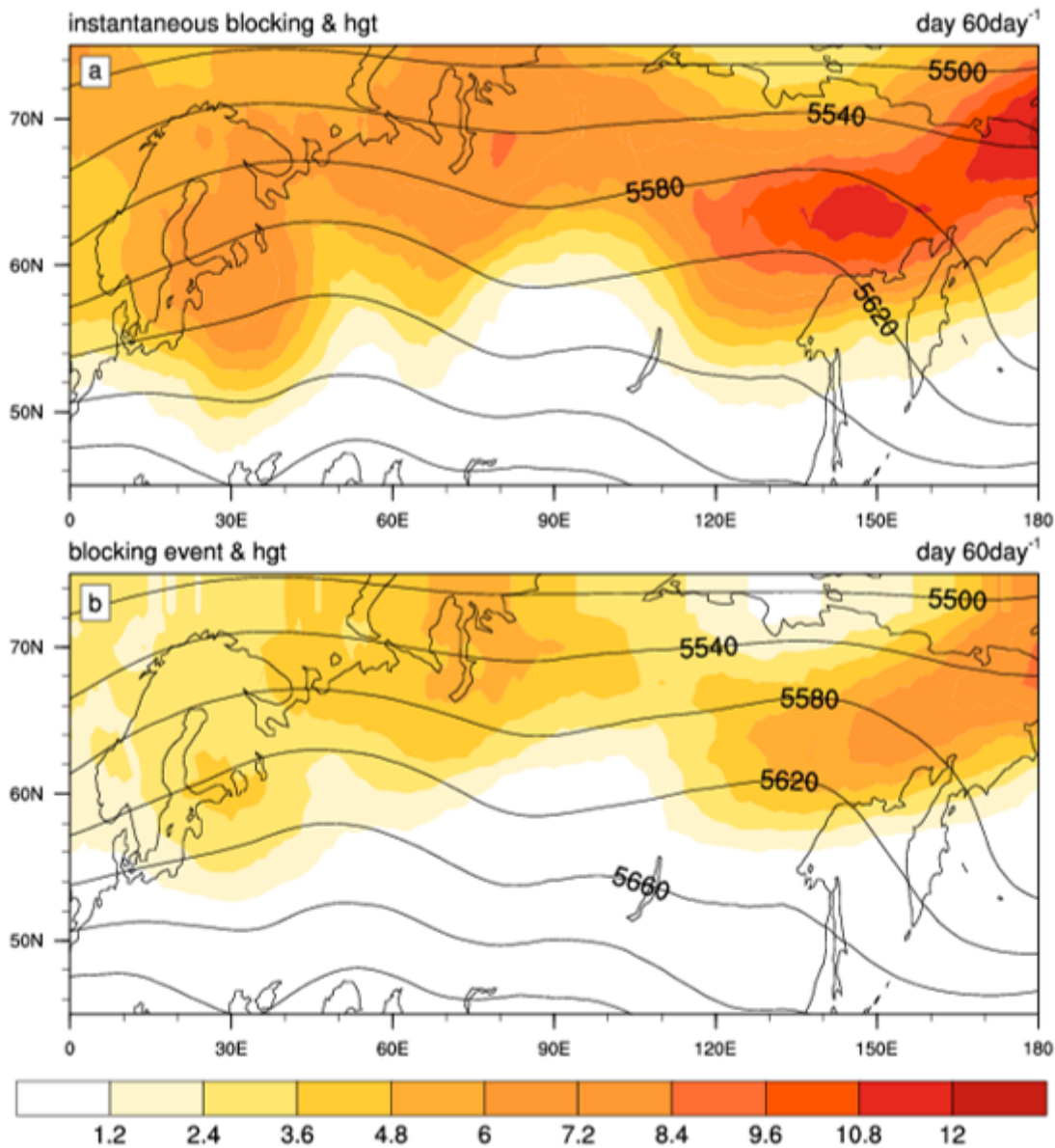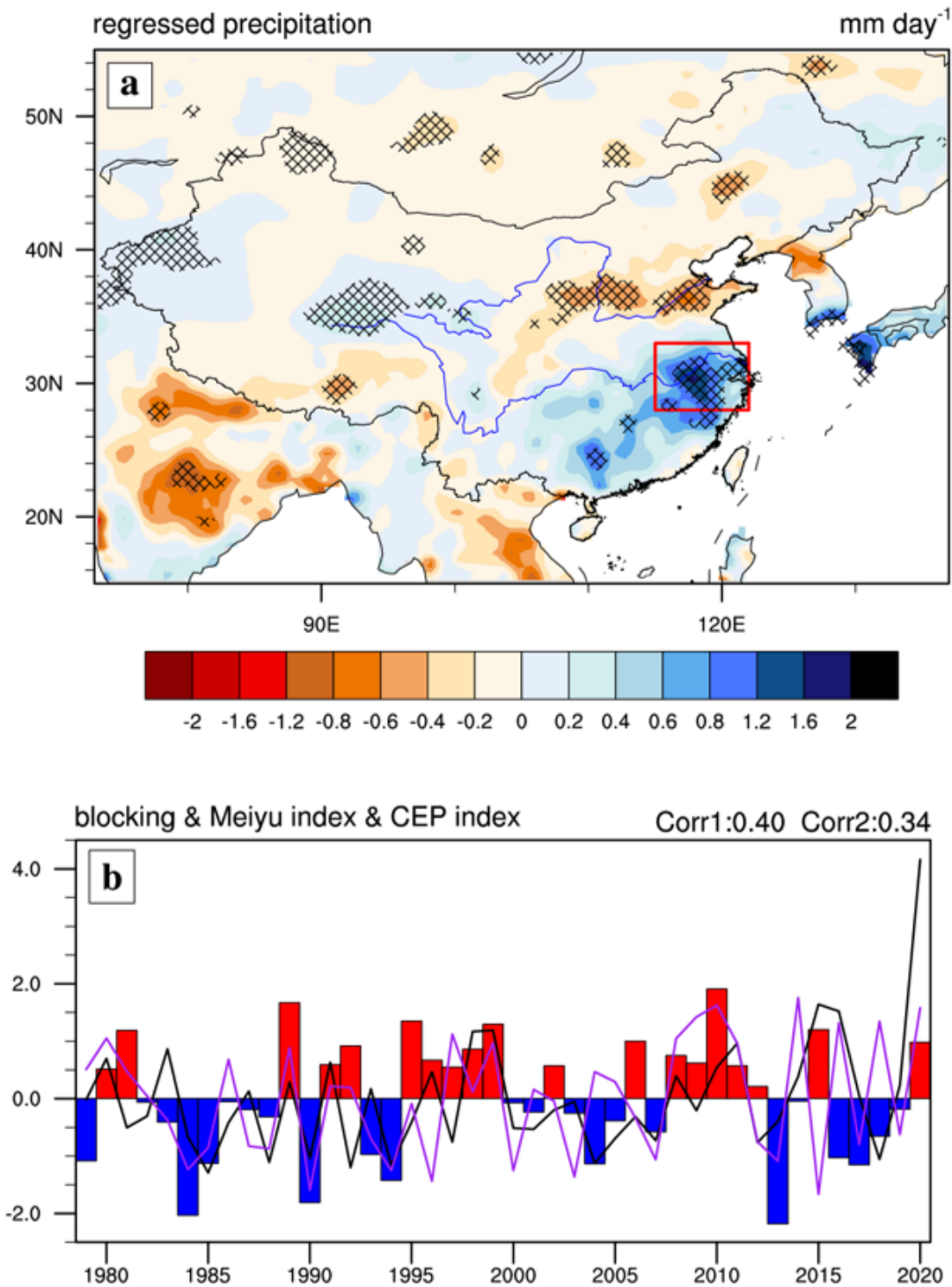
Figure 2

Horizontal distribution of Meiyu period climatological (a) instantaneous blocking frequency (units: day 60day^{-1}), (b) blocking events frequency (units: day 60day^{-1}). Black contours denote the climatology of 500 hPa geopotential height (units: gpm) during Meiyu period.

Figure 3

(a) Regressed Eurasian instantaneous blocking frequency (units: day 60day^{-1}) anomalies on the standardized time series of the 1st EOF mode. (b) Standardized time series (TPI) of the 1st EOF mode of Eurasian instantaneous blocking frequency for the period 1979-2020 during Meiyu period. Black contours of (a) are the same as that in Fig. 2, denoting the climatology of 500 hPa geopotential height (units: gpm) during Meiyu period.

Figure 4

(a) Regressed precipitation (shading; units: mm day^{-1}) anomalies during Meiyu period on TPI . (b) Time series of the Meiyu rainfall index (black line), the Central Europe precipitation index (purple line), and the TPI index (bar) for 1979-2020. Corr1 in (b) denotes the correlation coefficient between the Meiyu rainfall index and the TPI index, and Corr2 in (b) denotes the correlation coefficient between the Meiyu rainfall

index and the Central Europe precipitation index. The red box in (a) represents the Yangtze River valley. The crosses in (a) indicate the regions exceeding 95% confidence level with the Student's t-test.
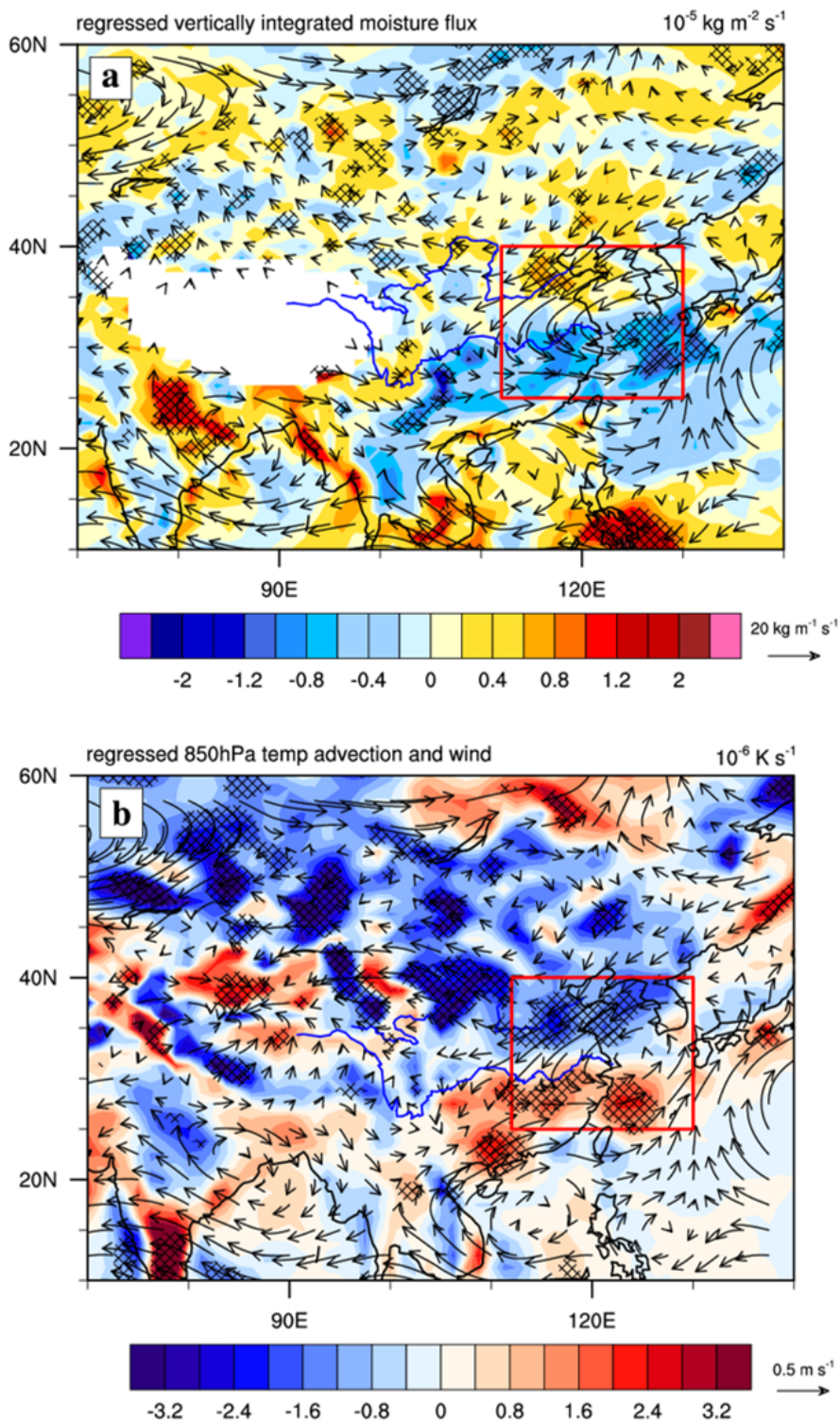
Figure 5

Regressed (a) vertically integrated water vapor fluxes (vectors; units: kg m^{-1} s^{-1}) and their divergence (shading; units: 10^{-5} kg m^{-2} s^{-1}), (b) 850 hPa temperature advection (shading; units: 10^{-6} K s^{-1}) and wind

(vector; units: m s^{-1}) anomalies on TPI during Meiyu period. The red box denotes the key region of eastern China. The crosses indicate the regions exceeding 95% confidence level with the Student's t-test.
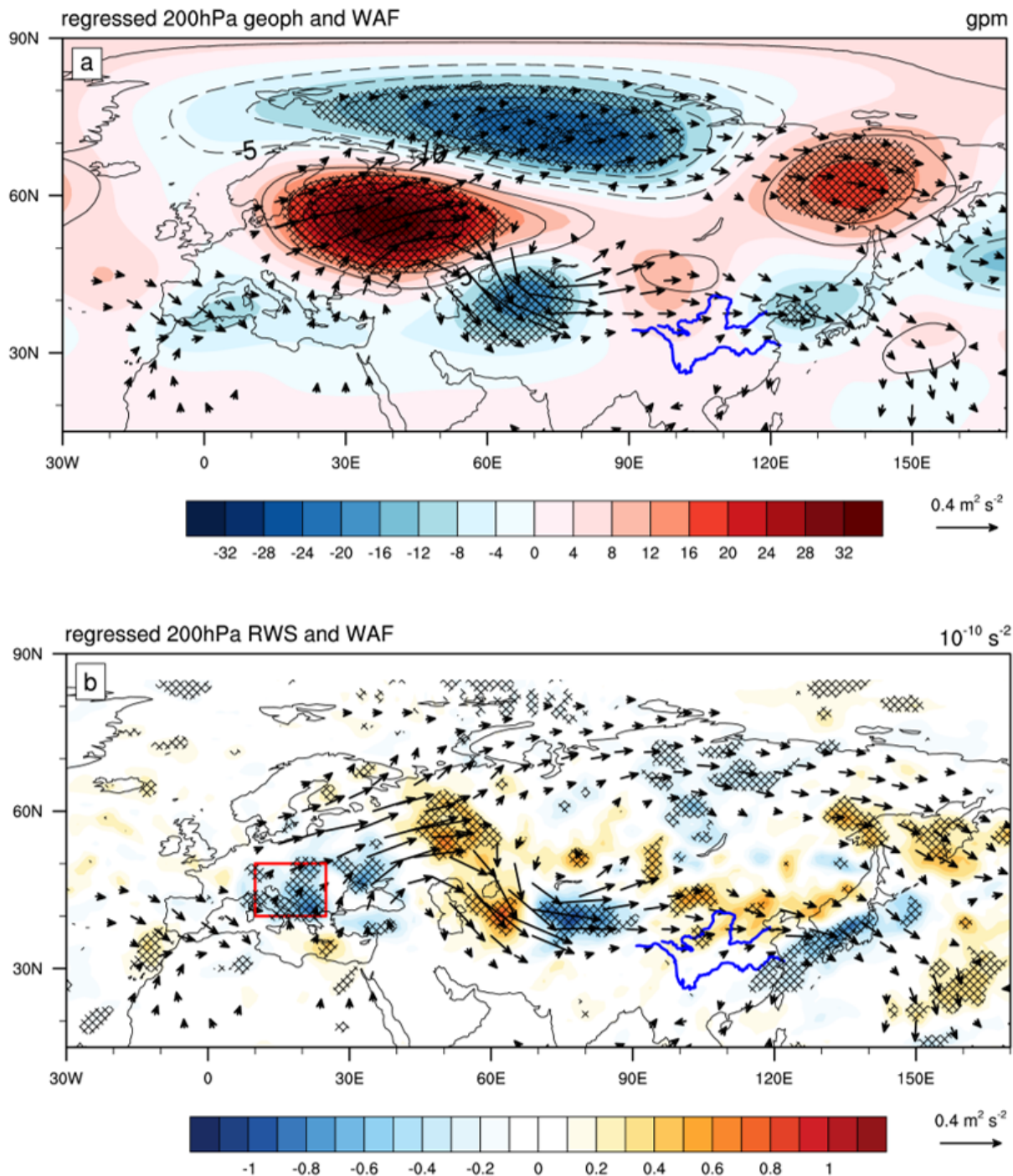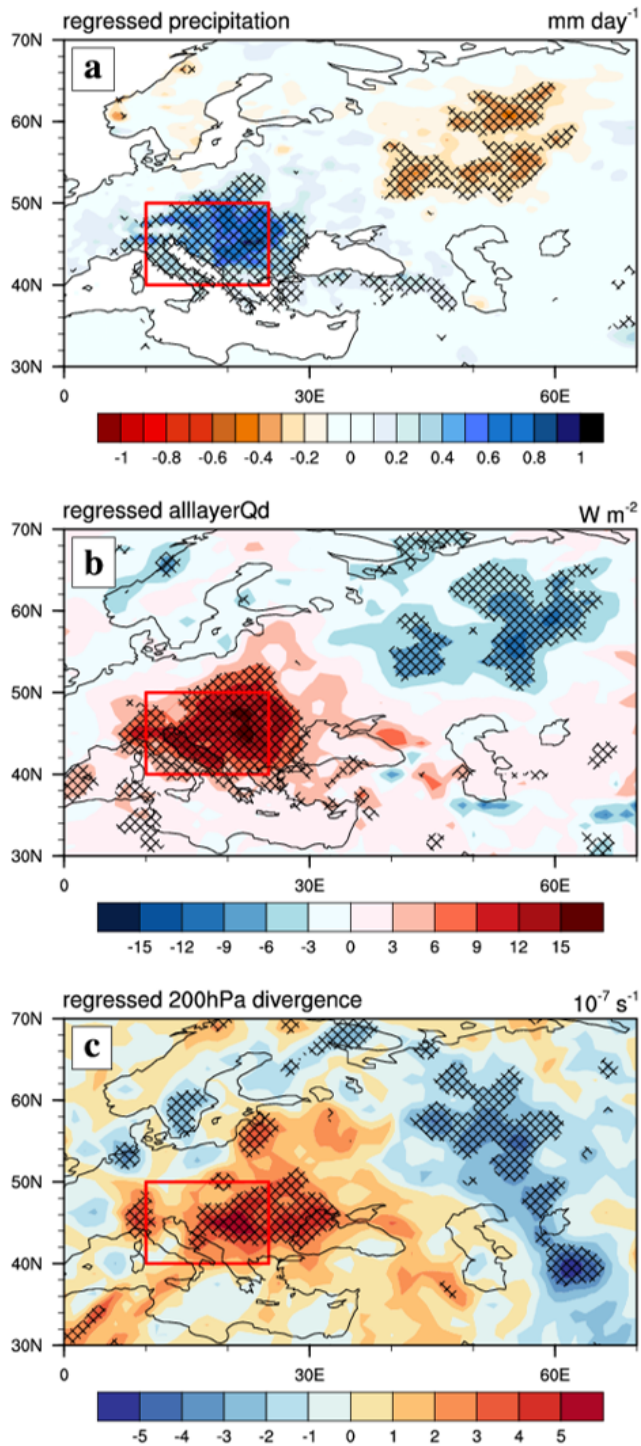

Figure 6

Regressed (a) 200 hPa (shaded) and 500 hPa (contours) geopotential height (units: gpm), (b) 200 hPa Rossby wave source (shading; units: 10^{-10} s^{-2}), and (a,b) 200 hPa WAF (vectors; units: m^2 s^{-2}) anomalies

on TPI during Meiyu period. The contour interval in (a) is 5 gpm from -20 gpm to 20 gpm. The red box in (b) denotes the region of the source of the Rossby wave. The crosses indicate the regions exceeding 95% confidence level with the Student's t-test.
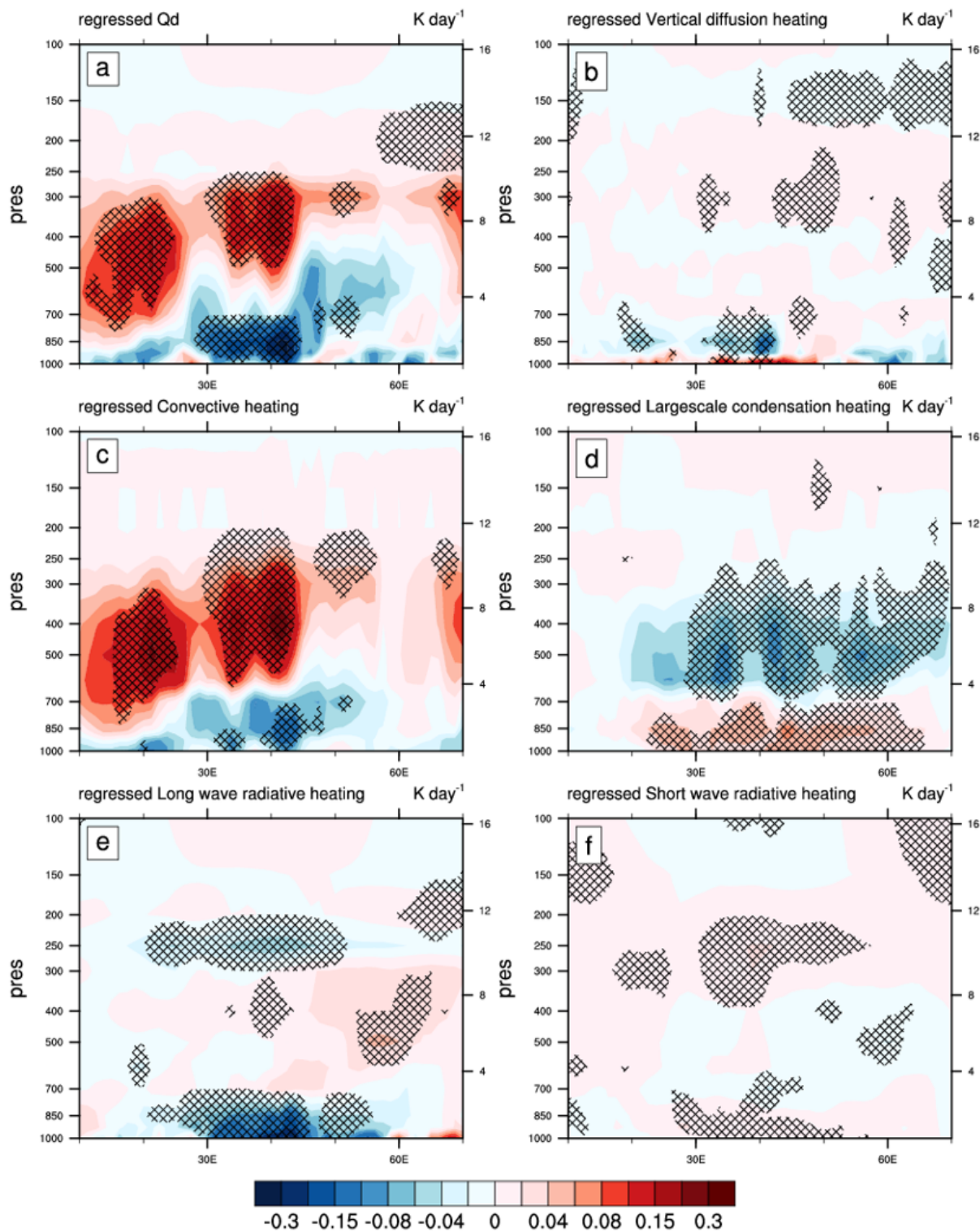
Figure 7

Longitude-altitude sections (averaged between 40°N and 50°N) of regressed (a) diabatic heating (units: K day^{-1}), and its component including (b) vertical diffusion, latent heat from (c) convective processes and (d) large-scale condensation, (e) longwave and (f) shortwave radiation anomalies on TPI during Meiyu period. The crosses indicate the regions exceeding 95% confidence level with the Student's t-test.
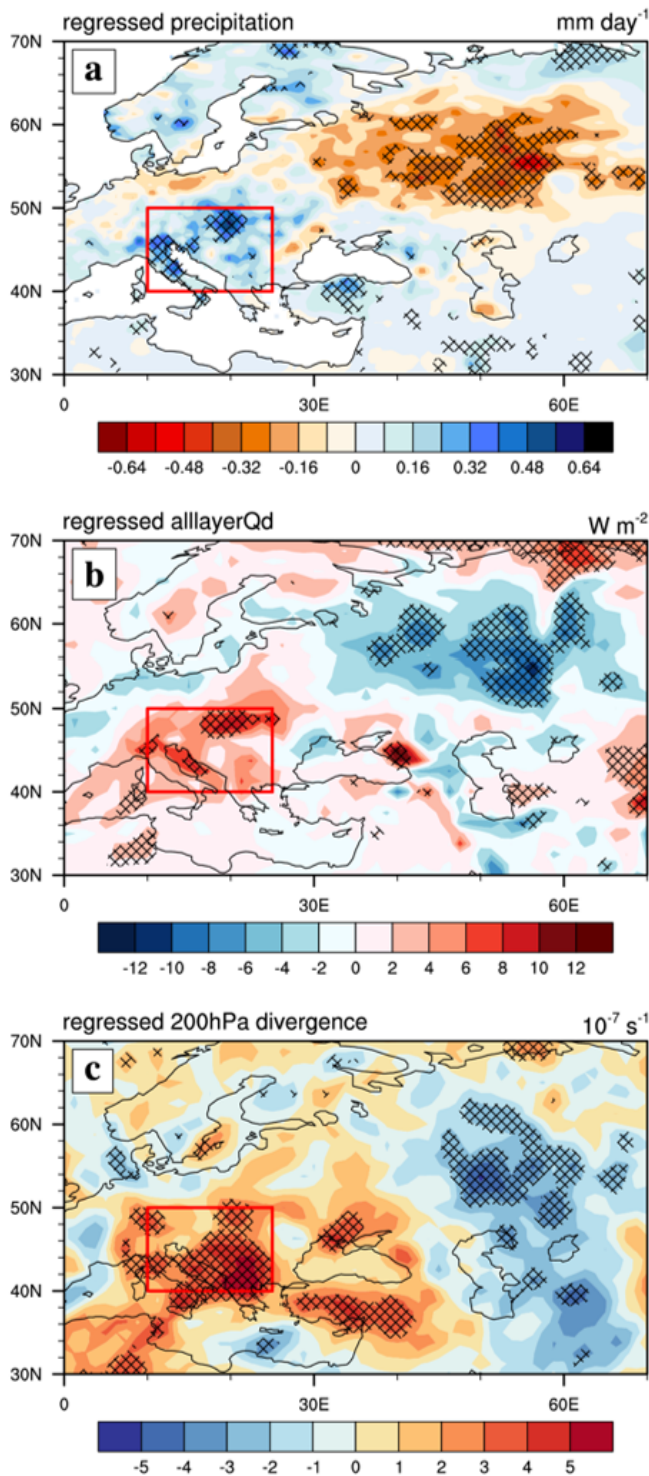
Figure 8

Regressed (a) precipitation (shading; units: mm day^{-1}), (b) 1000 hPa~100 hPa integrated diabatic heating (shading; units: W m^{-2}), (c) 200 hPa divergence (shading; units: 10^{-7} s^{-1}) anomalies on TPI during Meiyu period. The red box denotes the region of Central Europe. The crosses indicate the regions exceeding 95% confidence level with the Student's t-test.
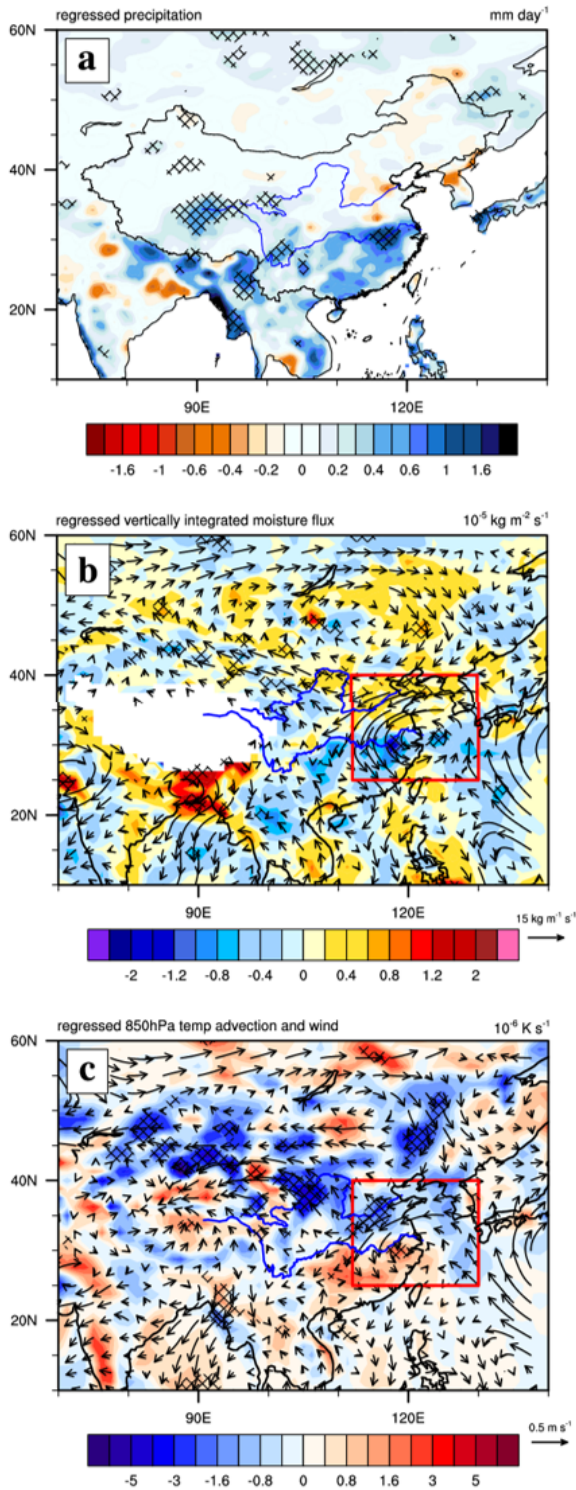

Figure 9

Regressed (a) precipitation (shading; units: mm day^{-1}), (b) 1000 hPa~100 hPa integrated diabatic heating (shading; units: W m^{-2}), (c) 200 hPa divergence (shading; units: 10^{-7} s^{-1}) anomalies on Central Europe precipitation index during Meiyu period. The red box denotes the Central Europe. The crosses indicate the regions exceeding 95% confidence level with the Student's t-test.
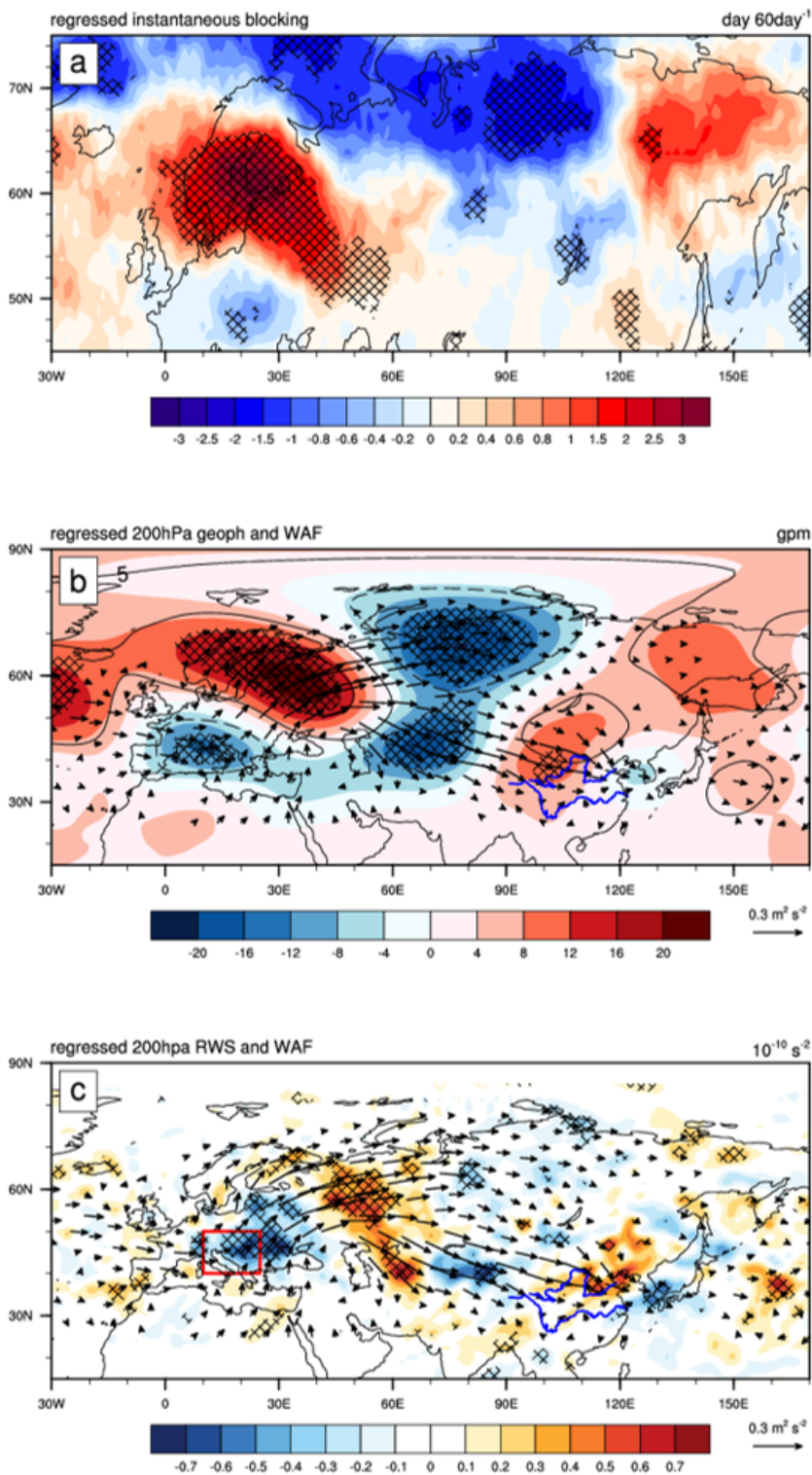
Figure 10

Regressed (a) instantaneous blocking frequency (shading; units: day 60day^{-1}), (b) 200 hPa (shading) and 500 hPa (contour) geopotential height (units: gpm), (c) 200 hPa Rossby wave source (shading; units:10^{-10} s^{-2}), and (b, d) 200 hPa WAF (vectors; units: m^2 s^{-2}) anomalies on the Central Europe precipitation index during Meiyu Period. The contour interval in (b) is 10 gpm from -15 gpm to 15 gpm. The red box in (c) denotes the Central Europe. The crosses indicate the regions exceeding 95% confidence level with the Student's t-test.
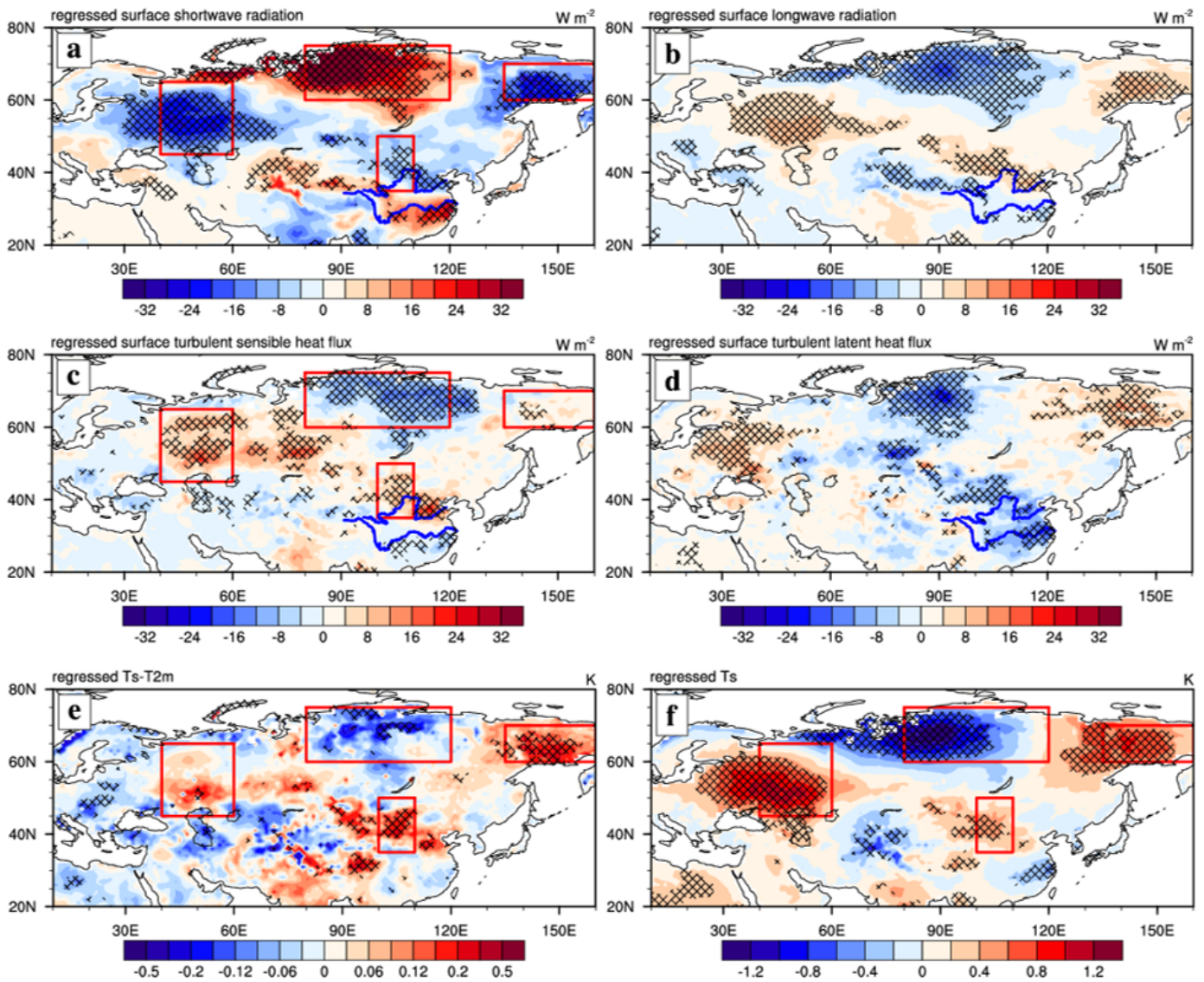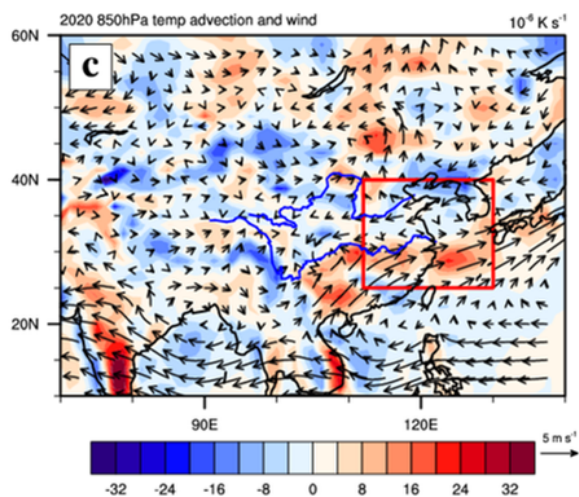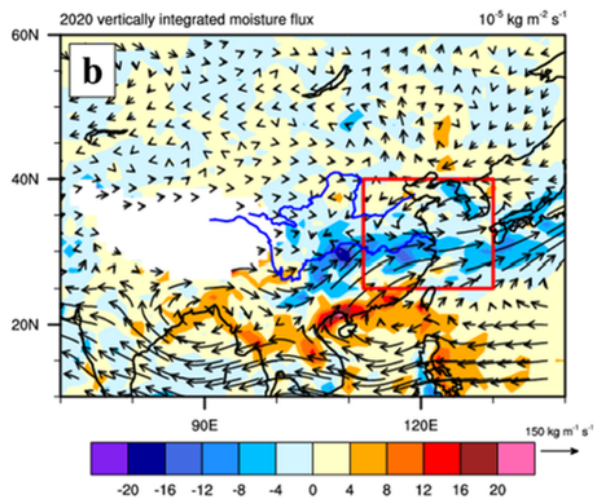
Figure 11

Regressed (a) precipitation (shading; units: mm day^{-1}), (b) vertically integrated water vapor fluxes (vectors; units: kg m^{-1} s^{-1}) and their divergence (shading; units: 10^{-5} kg m^{-2} s^{-1}), (c) 850 hPa temperature advection (shading; units: 10^{-6} K s^{-1}) and horizontal wind (vector; units: m s^{-1}) anomalies on the Central Europe precipitation index during Meiyu Period. The red box denotes the key region of eastern China. The crosses indicate the key regions exceeding 95% confidence level with the Student's t-test.
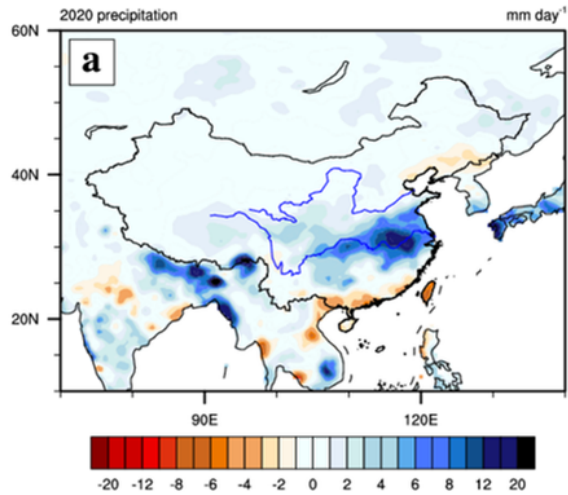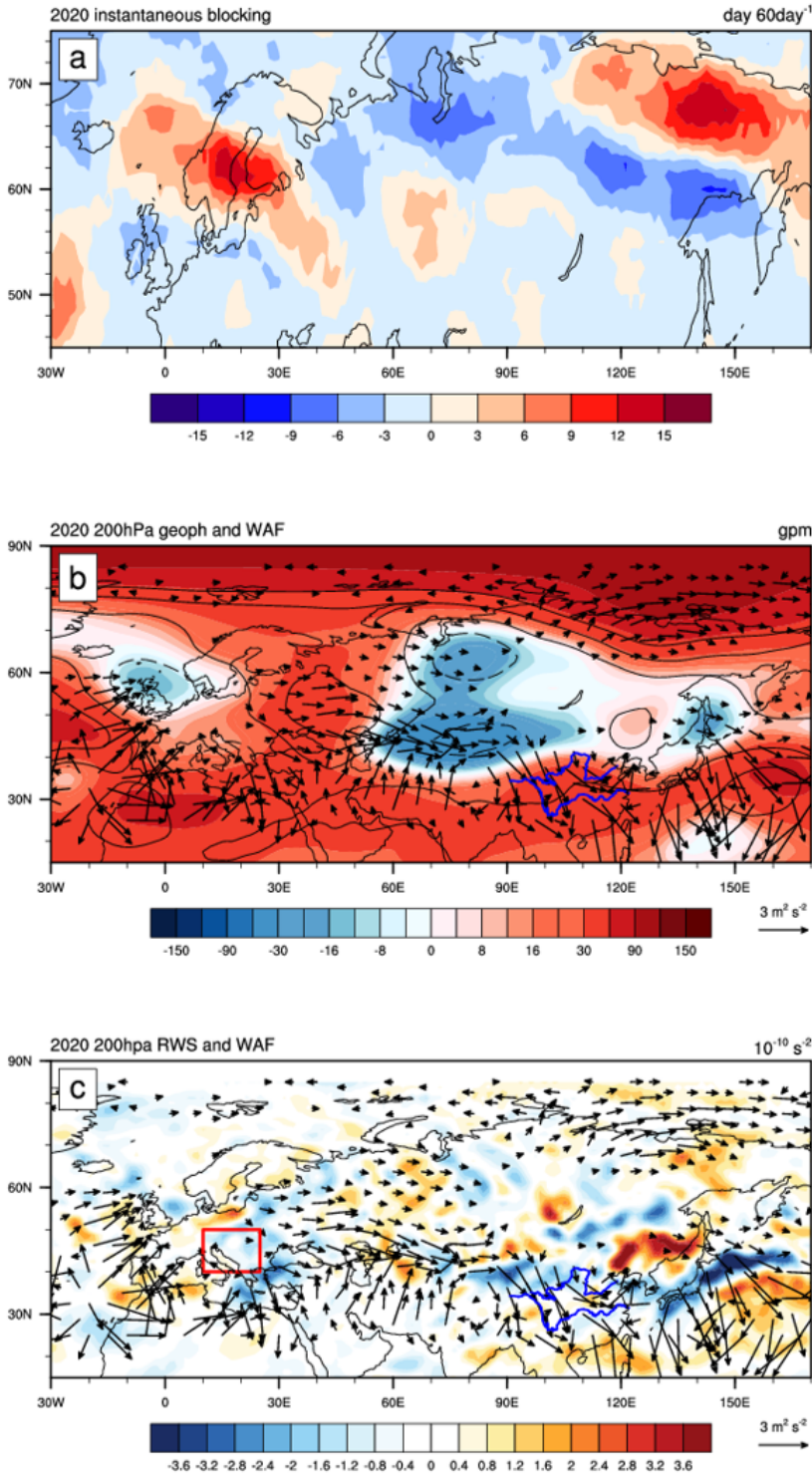

Figure 12

Regressed surface (a) shortwave and (b) longwave radiation (shading; units: W m^{-2}), turbulent (c) sensible and (d) latent heat flux (shading; units: W m^{-2}), (e) skin temperature minus air temperature at 2 m (shading; units: K), (f) skin temperature (shading; units: K) anomalies on TPI during Meiyu period. Positive indicates upward in (a-d). The red boxes denote Ural area, Siberian Plateau, Mongolia, and the Far East from leftmost to rightmost, respectively. The crosses indicate the regions exceeding 95% confidence level with the Student's t-test.
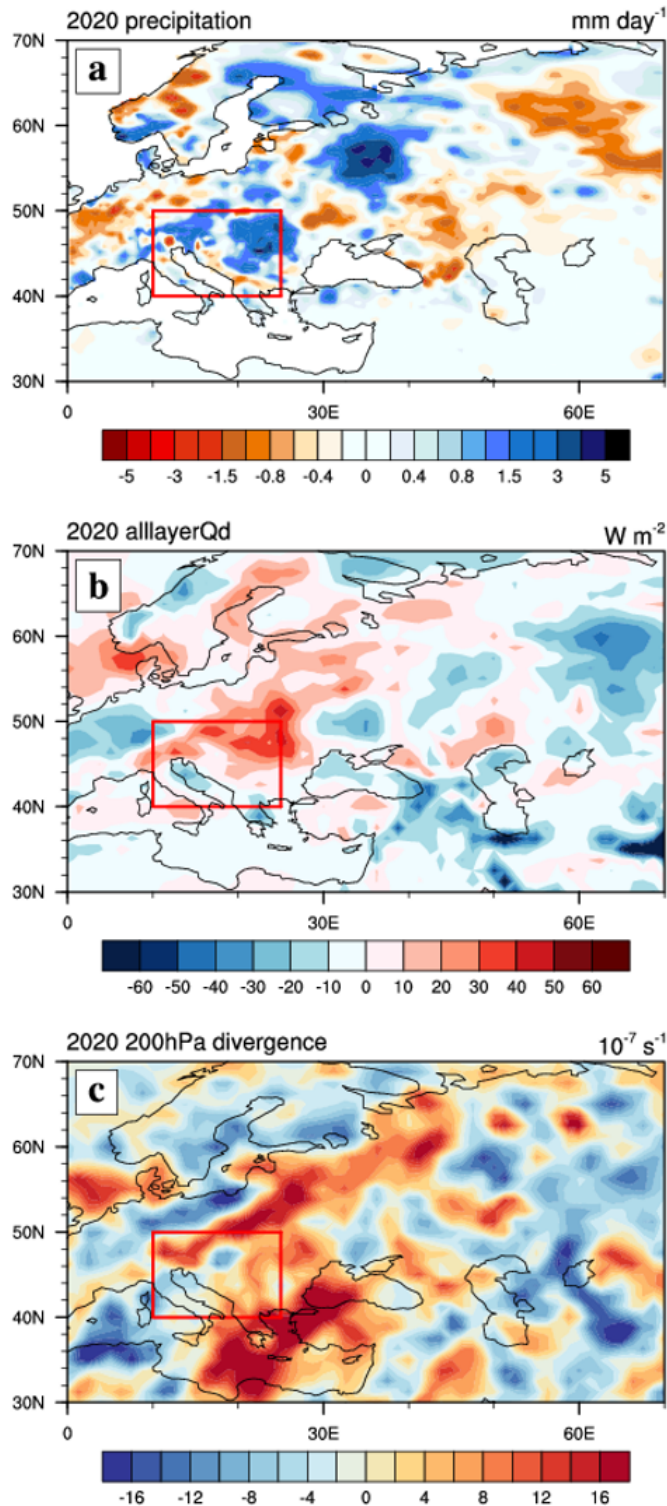
Figure 13

(a) Precipitation (shading; units: mm day^{-1}), (b) vertically integrated water vapor fluxes (vectors; units: kg m^{-1} s^{-1}) and their divergence (shading; units: 10^{-5} kg m^{-2} s^{-1}), (c) 850 hPa temperature advection (shading; units: 10^{-6} K s^{-1}) and horizontal wind (vector; units: m s^{-1}) anomalies during Meiyu period in 2020. The red box denotes the key region of eastern China.

Figure 14

(a) Instantaneous blocking frequency (shading; units: day 60day^{-1}), (b) 200 hPa (shading) and 500 hPa (contour) geopotential height (units: gpm), (c) 200 hPa Rossby wave source (shading; units:10^{-10} s^{-2}), and (b, d) 200 hPa WAF (vectors; units: m^2 s^{-2}) anomalies during Meiyu Period in 2020. The contour interval in (b) is 20 gpm from -50 gpm to 50 gpm. The red box in (c) denotes the Central Europe.

Figure 15

(a) Precipitation (shading; units: mm day^{-1}), (b) 1000 hPa~100 hPa integrated diabatic heating (shading; units: W m^{-2}), (c) divergence (units: shading; 10^{-7} s^{-1}) anomalies during Meiyu Period in 2020. The red box denotes the Central Europe.
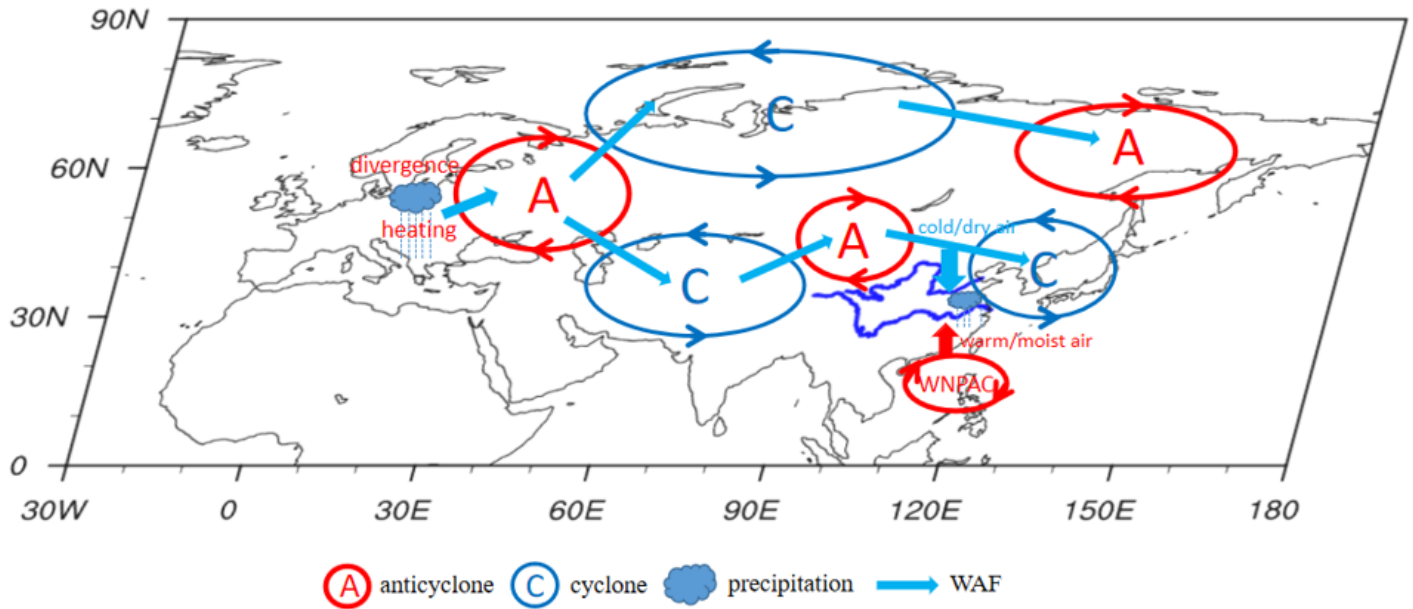
Figure 16

The schematic diagram to illustrate the physical processes associated with the tripole mode of the Eurasian blocking activities.